TEMPORAL VARIABILITY OF THE FLARE INDEX (1966–2001)

ATİLA ÖZGÜÇ[1], TAMER ATAÇ[1] and JÁN RYBÁK[2]
[1]*Boğaziçi University, Kandilli Observatory and Earthquake Research Institute, Çengelköy, 34684, Istanbul, Turkey (e-mails: ozguc@boun.edu.tr; atac@boun.edu.tr)*
[2]*Astronomical Institute, Slovak Academy of Science, Tatranská Lomnica, Slovak Republic (e-mail: choc@astro.sk)*

(Received 28 November 2002; accepted 28 January 2003)

Abstract. A brief description and study of the temporal variability of the flare index over the epoch of almost 4 cycles (1966–2001) are presented. Using Fourier and wavelet transforms the long- and the intermediate-term periodicities in the daily flare index data for the total surface and for the northern and the southern hemispheres of the Sun are given in detail. A significant variability was found for all periods including those of 150 days and 1.3 years. The wavelet transform results show that the occurrence of flare index power is highly intermittent in time. A comparison of the results of the Fourier transform and the time-period wavelet transform of the flare index time series has clarified the importance of different periodicities, whether they are or are not the harmonics of the basic ones, as well as the temporal location of their occurrence.

1. Introduction

Solar activity variations exhibit themselves in electromagnetic radiation from radio frequencies of a few kHz to powerful gamma rays and also in particle flux. Images of the Sun show that solar flares are one of the most powerful and explosive of all forms of solar activity. Many studies in the solar terrestrial field classified solar flares as one of the most important solar events affecting the Earth as are coronal mass ejections (CMEs). The long-term evolution of solar activity, on time scales of the solar cycle and beyond, has been studied from different perspectives using a variety of short and long-term solar activity indicators. The gamma-ray spectrometer aboard the Solar Maximum Mission discovered a 154-day periodicity in solar flare rates (Rieger *et al.*, 1984). Subsequently, periodicities in various flare activities and in sunspot areas or groups during a few years around solar maxima have been extensively monitored using different diagnostics and at many electromagnetic wavelengths (see, e.g., for X-ray flares, Dennis, 1985; Bai and Sturrock, 1987; for flares producing energetic interplanetary electrons, Dröge *et al.* 1990; for type II and IV radio bursts, Verma *et al.*, 1991; for microwave peak flux, Bogart and Bai, 1985; for flare index, Özgüç and Ataç, 1989, 1994; Özgüç, Ataç, and Rybák, 2002; for sunspot area, Lean and Brueckner, 1989; Oliver, Ballester, and Baudin, 1998; and for sunspot numbers, Ballester, Oliver, and Baudin, 1999). The origin of such quasi periodicities, particularly prominent during solar maxima, has

Solar Physics **214:** 375–396, 2003.

remained a mystery for nearly two decades. In this study the solar flare index (FI) variability is examined using the data for almost 35.5 years. Long-term observations of solar activity indicate that each hemisphere's solar activity is obviously statistically different from that of others. Therefore both hemispheres and the total visible surface of the Sun are examined separately to confirm the existence of solar activity periodicities as well as to show the north–south asymmetry phenomenon.

The presence of periodicities in FI has been analyzed before for individual cycles by Özgüç and Ataç (1989, 1994). They have examined the periodicities for the cycles 20, 21, and 22 and have found 152- and 564-day periodicities for cycles 20 and 21. The same analysis has been done for cycle 22 and instead of a 152-day periodicity, 53- and 73-day periodicities were found. Özgüç, Ataç, and Rybák (2002), have studied the existence of the intermediate-term periodicities for the rising part of cycle 23. They considered the FI for the data period from 1 June 1996 to December 31, 2000 and found that 35-, 62-, 116, 198-, and 276-day periodicities are in operation. Contrary to the previous three cycles 155-, 73-, or 51-day periodicities were not detected in this branch of the cycle.

To estimate periodicities the discrete Fourier transform (FT) was employed for the whole FI data set used in this paper. Since the commonly used FT is not able to disclose the possible changes in the periodicities over the period studied, the wavelet transform (WT) was applied to search for temporal variability. In Section 2 we specify the data used and describe the methods of analysis. Results and discussion are given in Sections 3 and 4, respectively.

2. Data and Methods of Analysis

2.1. Solar flare index

Solar activity can be measured at various heights in the solar atmosphere and these measurements can be compared with observed changes in the heliosphere. In this paper, we have considered the FI for the period data from 1 January 1966 to 1 July 2001 (total 12965 days). The quantitative flare index first introduced by Kleczek (1952), $Q = it$, may be roughly proportional to the total energy emitted by the flare. In this relation, i represents the intensity scale of importance of a flare in Hα and t the duration in Hα (in min) of the flare. Table I lists values of i used for the determination of Q. The daily sums of the index for the total surface are divided by the total time of observation of that day. Because the time coverage of flare observations is not always complete during a day (sometimes 75% or 90%), it is corrected by dividing by the total time of observations of that day to place the daily sum of the flare index on a common 24-hour period. The daily total time of observation is calculated from *Solar Geophysical Data Comprehensive Reports*. Calculated values are available for general use in anonymous ftp servers of our

TABLE I
Values of i used for the determination of FI.

Importance	i	Importance	i
SF, SN, SB	0.5	2B	2.5
1F, 1N	1.0	3F, 3N, 4F	3.0
1B	1.5	3B, 4N	3.5
2F, 2N	2.0	4B	4.0

observatory[1] and National Geophysical Data Center (NGDC)[2] This data set constitutes almost 35.5 years (see Figure 1). The flare index is an interesting parameter and is of value as a measure of the short-lived activity on the Sun and allows us to study long- and intermediate-term variation of the Sun. Obtained results (e.g., Li *et al.*, 2002; Kane, 2002; Joshi, 2001; Tripathy *et al.*, 2000; Veretenenko and Pudevkin, 1999) have shown that FI data may be used to study solar activity and its relation with the other activity indicators as well as the heliospheric changes. Therefore this two-dimensional index is physically good enough to describe the flare activity; because there are no limitations to compile it. Recently, Caballero and Valdés-Galicia (2001) reported that as for the case of the sunspot number, the solar FI data are stationary. This is not a surprise, because some authors (Özgüç, Tulunay, and Ataç, 1998; Özgüç *et al.*, 1998) have already used FI instead of sunspot numbers to study ionospheric variations. Since use of FI in various studies is increasing, two of the authors (A.Ö. and T.A.) will continue to compile this index in the future. To improve the FI any idea which makes it better in describing flare activity is welcome.

2.2. Discrete Fourier Transform

The search for periodicities in all the time series was performed by calculating the discrete Fourier transform. This technique indicates which periodicities are in operation during the studied period, which covers about 12965 days. We examined three FI time series, which are for the total surface and for the northern and the southern hemispheres, by computing the periodograms after tapering 5% of the data at the ends of the time intervals by applying a split bell cosine window (Bloomfield, 1976). These three time series are smoothed with 7-day running means only when the long-term periodicity is sought. Figures 2–4 (left panels) show the normalized power spectra of the three time series for the three period intervals of 1500–500, 500–100, and 100–30 days, respectively. For these figures the power spectra were calculated for the 8–23, 23–116, and 116–386 nHz ranges with 0.89 nHz intervals.

[1] *ftp://ftp.koeri.boun.edu.tr/pub/astronomy/flare_index.*
[2] *ftp://ftp.ngdc.noaa.gov/STP/SOLAR_DATA /SOLAR_FLARES/INDEX.*

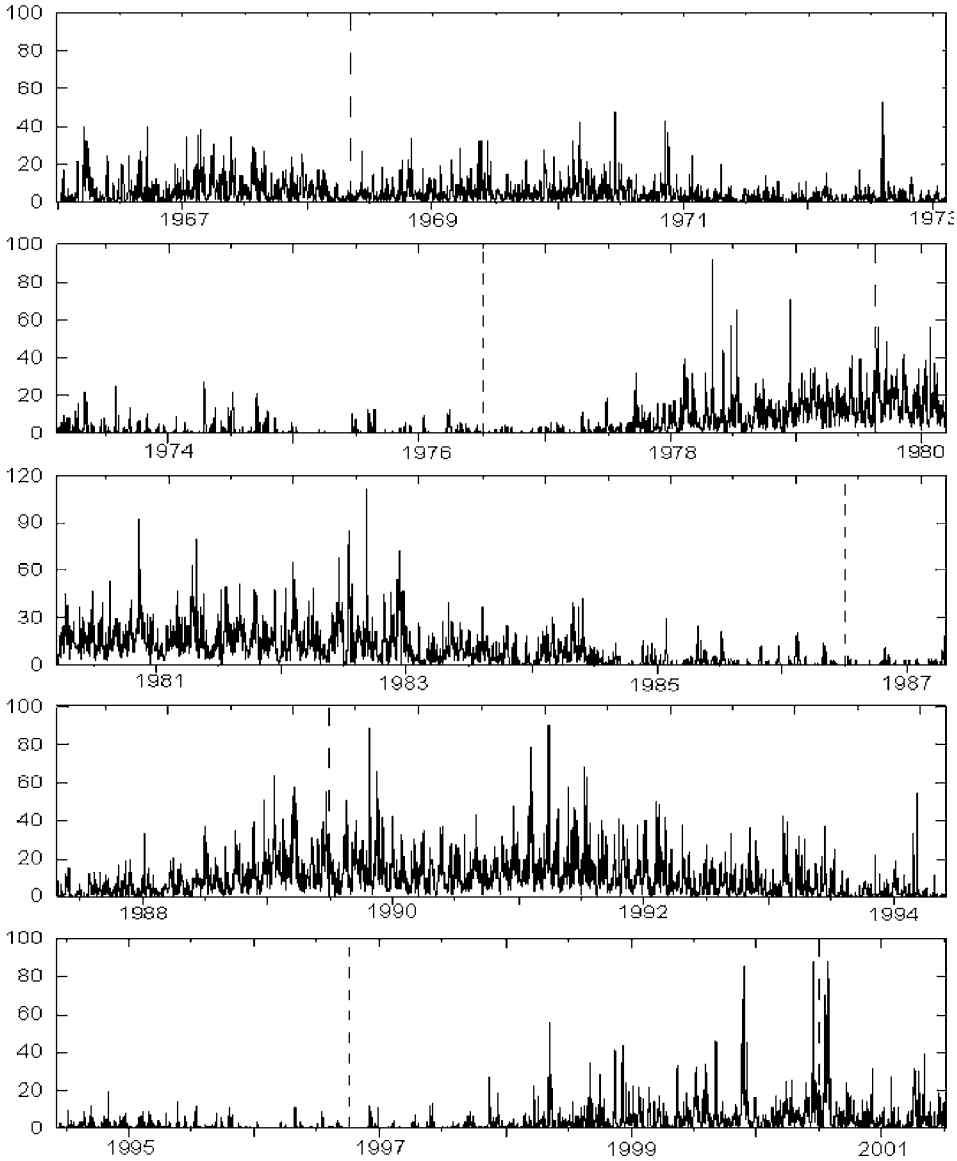

Figure 1. Behavior of the FI daily values for the cycles 20–22 and first half of cycle 23. *Long* and *short dashed vertical lines* mark the solar activity cycle maxima and minima, according to NOAA's mean monthly sunspot numbers, respectively.

TABLE II

Periodicities found by Fourier power spectral analysis. P, F, and R show periods given in days, the false alarm probability (FAP) values, and the probability values after randomization of time series, respectively.

Total surface			Northern hemisphere			Southern hemisphere		
P	F (%)	R (%)	P	F (%)	R (%)	P	F (%)	R (%)
53	5.4	6.3	–	–	–	54	5.3	8.5
75	18.0	20.2	73	4.0	8.3	75	9.2	7.5
84	14.0	7.8	85	12	6.8	–	–	–
–	–	–	–	–	–	116	4.0	7.8
147	3.7	2.0	–	–	–	–	–	–
–	–	–	205	4.9	7.1	–	–	–
–	–	–	301	17.0	8.9	316	9.5	15
–	–	–	498	2.1	0.9	510	7.5	5.7
–	–	–	544	3.7	6.7	539	5.9	9.0
618	26.0	21.8	–	–	–	661	7.9	4.3
–	–	–	–	–	–	780	14.1	20.7
1153	4.5	8.0	–	–	–	–	–	–

The uncertainty in each frequency is ± 0.4 nHz due to the 37-year data length. There are several significant peaks in these figures whose statistical significances and probabilities of the obtained high peaks are listed in Table II.

The flare index is not statistically independent but is correlated with a characteristic correlation time of a week. Therefore the power distribution follows an exponential distribution (Horne and Baliunas, 1986); i.e., the probability of the power density at a given frequency being greater then k by chance is given by

$$P(z > k) = \exp(-k/\sigma^2), \tag{1}$$

where the normalization factor k, should be determined empirically (Delache, Laclare, and Sadsaoud, 1985; Bai and Cliver, 1990; Bai, 1992). Even if we use a normalized time series

$$X_{ii} = (X_i - X_{av})/\sigma,$$

where X_i is the Q value on the ith day, X_{av} is the daily mean flare index value, and σ is the variance, because of the interdependence of occurrence of some big flares, the Fourier periodogram turns out to be not normalized. Therefore, whatever analysis method is used, the best way to normalize the power spectrum is to fit the actual power distribution to Equation (1) (Bai and Cliver, 1990). Figures 2–4 right panels show the distribution of the Fourier power values corresponding to the normalized spectra shown in Figures 2–4 (left panels). The vertical axes

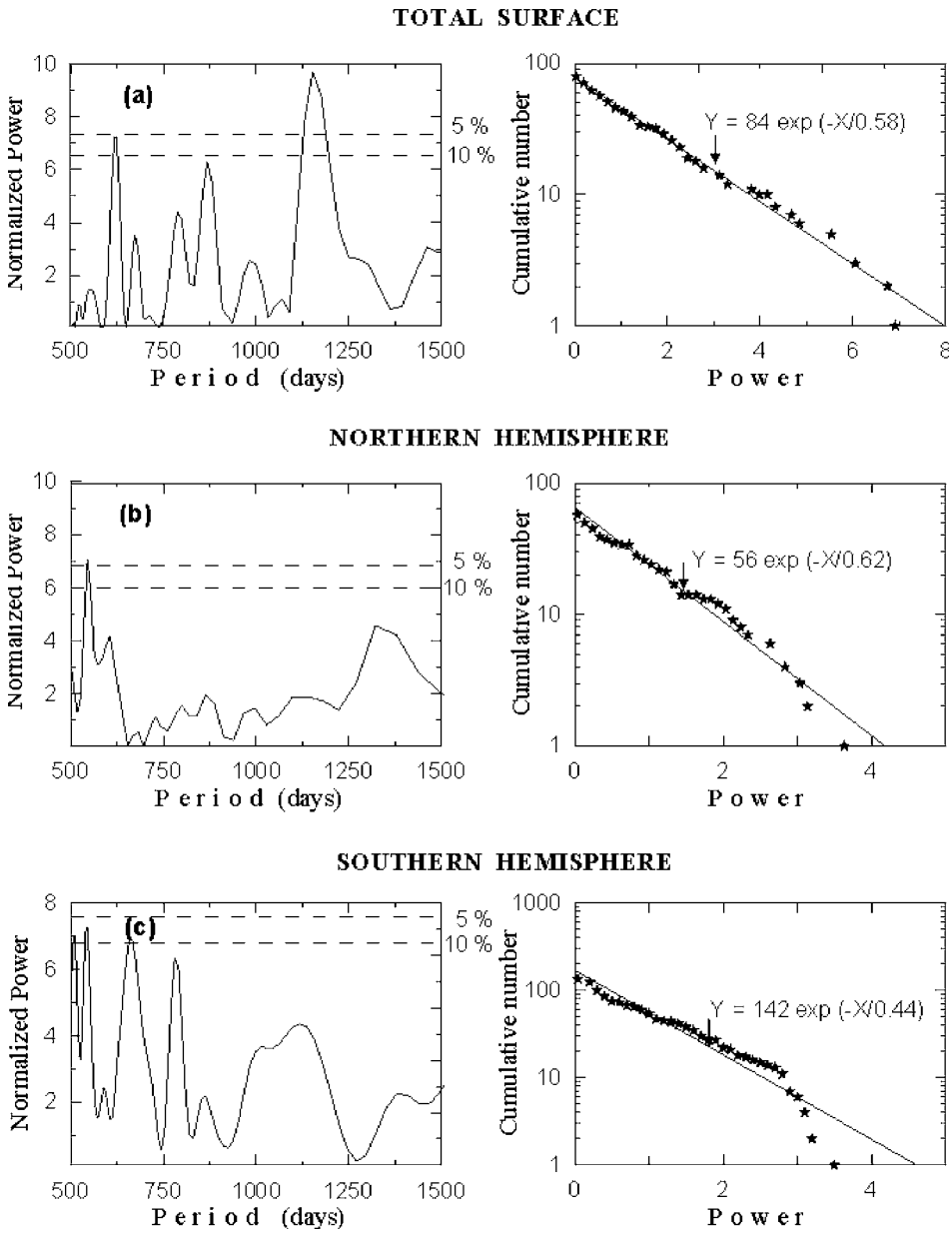

Figure 2. Normalized power spectra of the flare index (*left panel*) and power distribution of discrete Fourier transform (*right panel*) of (a) the total surface of the Sun, (b) the northern hemisphere, and (c) the southern hemisphere for time interval of 12950 days and for period interval of 500–1500 days. The *dashed lines* in the left panels indicate the FAP significance levels. The *vertical axes* of the right sides are the numbers of frequencies for which power exceeds X. The *straight lines* are the fit to the points for lower values of power.

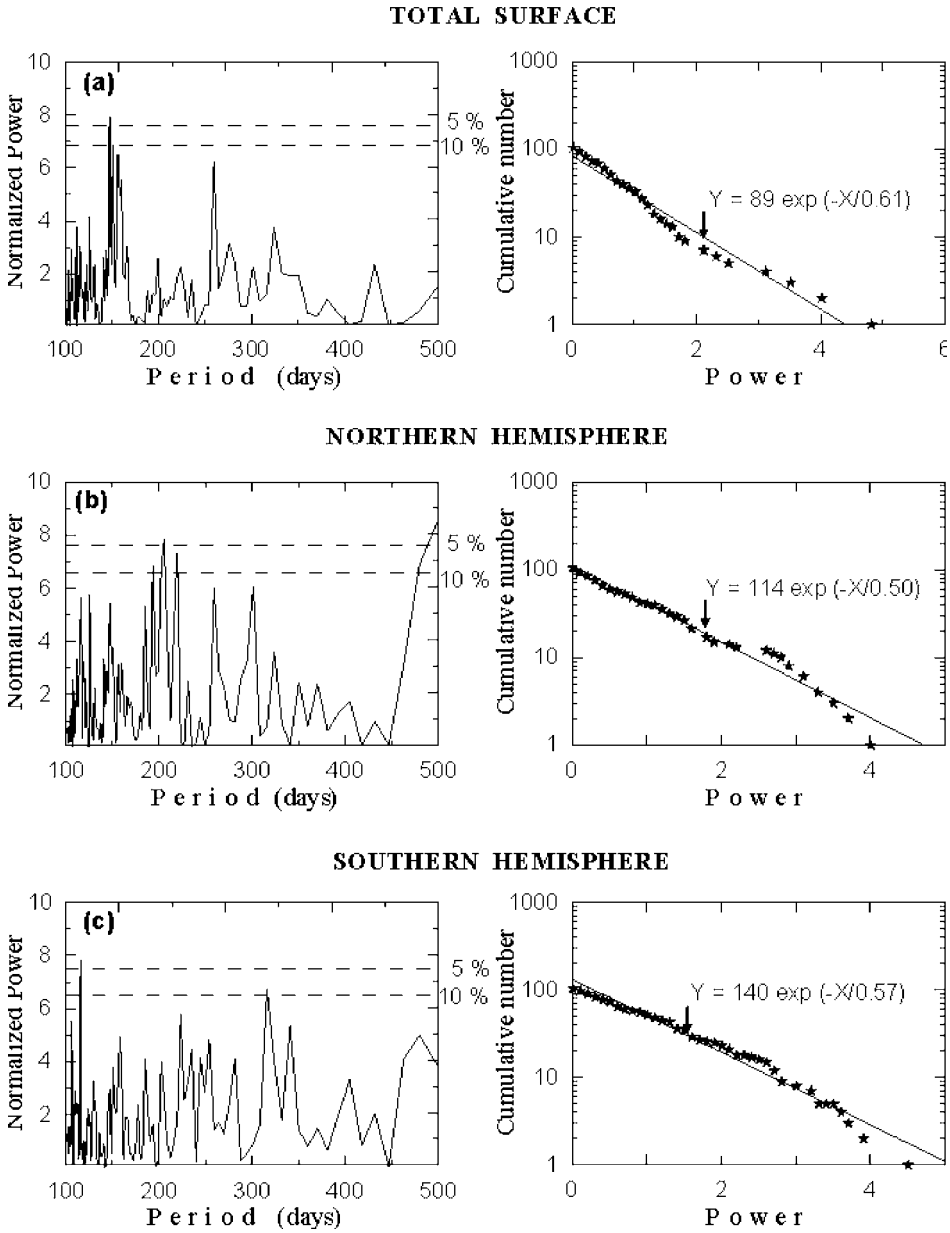

Figure 3. Same as Figure 2, but for the period interval of 100–500 days.

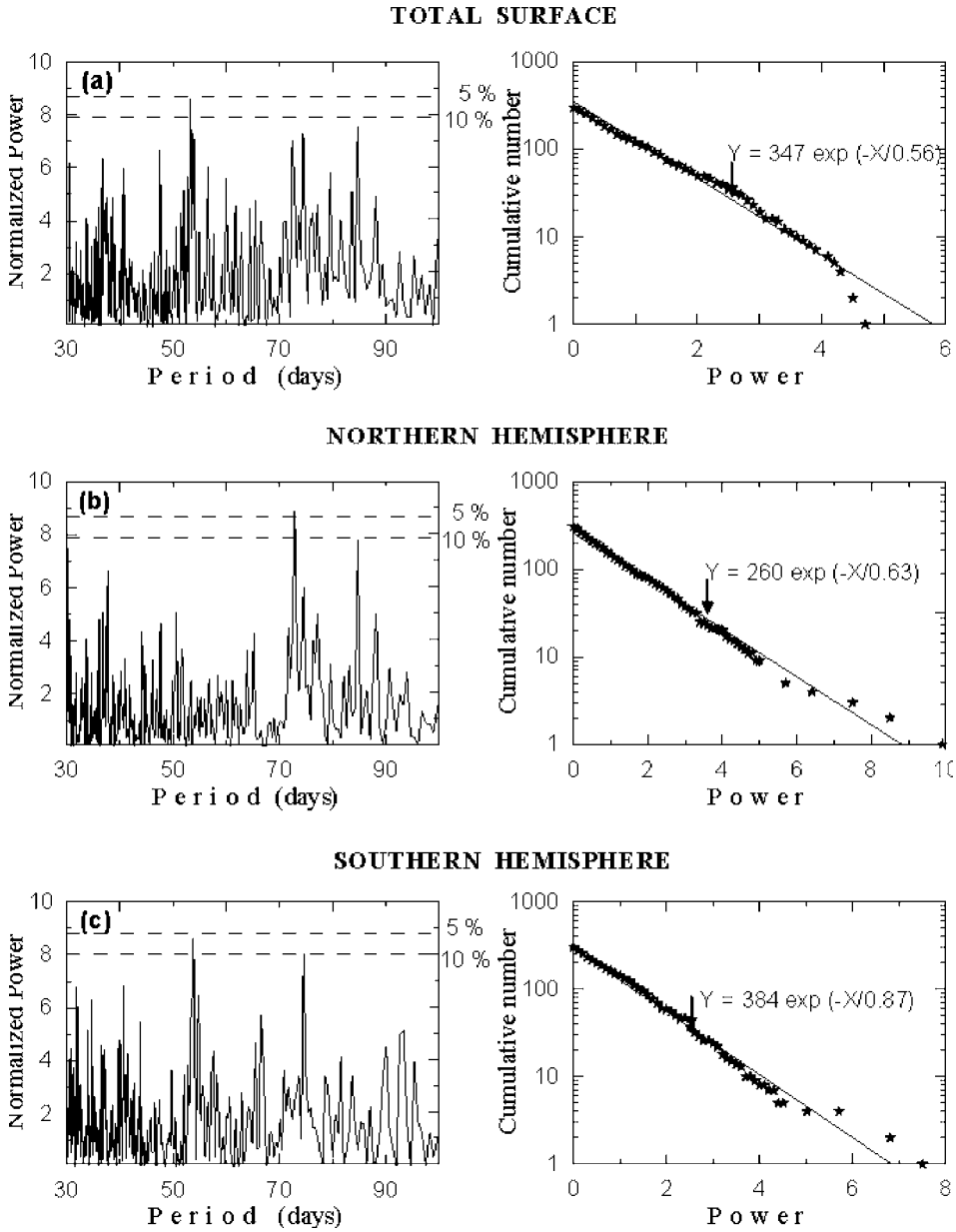

Figure 4. Same as Figure 2, but for the period interval of 30–100 days.

show the cumulative number of frequencies for which the power exceeds a certain value; of course for all frequencies the power exceeds zero. At only one or two frequencies are the powers at their maximum values. For lower values of power, the distributions can be well fitted by the equations which are shown in the Figures 2–4 (right panels), as expected from Equation (1). Thus, we normalize the power spectrum by dividing the powers by these k factors to obtain Figures 2–4 (left panels). Once the power spectra have been properly normalized (which means that the constant k in Equation (1) has been computed for each spectrum and the power spectra divided by k) we can use the 'false alarm-probability' (FAP) formula to estimate the statistical significance of a peak in the power spectrum. The FAP is given by

$$F = 1 - [1 - \exp(-Z_m)]^N, \tag{2}$$

where Z_m is the height of the peak in the normalized power spectrum and N is the number of independent frequencies (Scargle, 1982; Horne and Baliunas, 1986). If we have a discrete power spectrum giving the power at each of N independent frequencies for a set of random data, then F indicates the probability that the power at one or more of these frequencies will exceed Z_m by chance.

Fourier components calculated at frequencies at intervals of the independent Fourier spacing (ifs), $\Delta f_{\text{ifs}} = \tau^{-1}$, where τ is the time span of the data, are totally independent (Scargle, 1982). However, de Jager (1987) has shown by Monte-Carlo simulations that the Fourier powers taken at intervals of one-third of the independent Fourier spacing are still statistically independent. For $\tau = 12965$ days $\Delta f_{\text{ifs}} = 0.89$ nHz. Thus, there are 17, 104, and 303 independent frequencies in the 8–23, 23–116, and 116–386 nHz intervals, respectively (according to de Jager (1987), 51, 312, and 909 independent frequencies, respectively). The FAP is calculated for each peak as follows: if we take the height of the peak and the number of independent frequencies (17) in Figure 2(a) for the total surface, and substitute them in the FAP's expression, we would underestimate the FAP (in our case we would obtain 0.9%). However, when substituting $N = 80$ we compensate the effect of the increase of the peak value by oversampling. The oversampling tends to estimate more accurately the peak value. Therefore, if we substitute $Z_m = 7.46$ and $N = 80$ (since we searched 80 frequencies with 0.89 nHz intervals) in Equation (2) we get the false alarm probability $F = 0.045$; i.e., the probability to obtain such a high peak by chance is about 4.5%. The same analysis has been applied to the corresponding time series and the results can be seen in Table II.

Since peaks in a periodogram may arise from aliasing or other phenomena not present in gaussian noise (e.g., spectral leakage arising from the spacing of the data and from the finite length of the time series), the FAP criterion, alone, is insufficient for establishing whether or not a strong peak in a periodogram is indeed a real periodicity in the time series. To ensure that a periodicity suggested by a strong peak in the periodogram is not spurious, we have recomputed the periodograms after randomizing the data on the time grid. This procedure (Delache, Laclare,

and Sadsaoud, 1985) destroys coherent signals in the time series, but preserves the window and noise characteristics. Before randomizing, we have to consider the effect of flare clustering. We first cut the data with intervals varying from 20 to 40 days, and then shuffle them to obtain a randomized data set. Then we calculate the power of the randomized data set at the number of independent frequencies in the three frequency intervals, which we searched. We repeat these simulations 1000 times for each time series, every time computing the number of cases in which the recalculated power values for the periods having peaks in the original spectrum equal to or larger than the peaks power of the real data. The results of these calculations are presented in Table II. After inspection of this table, the results of these analyses give us confidence that the peaks in Figures 2–4 arise from coherent signals. Although there are some differences between FAP and randomizing test results, they may arise from the selected randomizing method, which yields insufficient randomizing in some cases.

2.3. WAVELET ANALYSIS

Classical Fourier transform analysis (FT) allows the study of a signal only in the frequency domain, whereas wavelet transform (WT) analysis yields information in both time and frequency domains (e.g., Daubechies, 1990; Kumar and Foufoula-Georgiou, 1997). Due to the past findings related to the intermittent behavior of the intermediate-term periods, we have also applied wavelet analysis to the three time series (total, north, south) consisting of daily flare index between 1 January 1966 and 1 July 2001 to study the temporal variation of periods. These three time series were smoothed with 7-day running means before the WT calculations. The algorithm of the continuous wavelet transform was applied after Torrence and Compo (1998) within the period ranges 20–100, 100–500, and 500–1500 days. The Morlet wavelet, a plane sine wave with amplitude windowed in time by a Gaussian function, has been selected to search for variability at different frequencies over the whole length of the time series. The non-dimensional frequency has been set to 6 fixing the length of all wavelets according to their scale. The used period resolution was changing from 0.5 to 2.9, 1.5 to 11.5, and 5.5 to 57 days, respectively. The calculated wavelet power is suppressed on the edges of the time domain due to the applied WT algorithm within the cones of incidence located at the temporal edges of the domain (indicated in our plots by cross-hatched regions). The significance levels of the calculated WT power were derived using the null hypothesis according to Torrence and Compo (1998) assuming noise distributed independently on periods. The 95% confidence level, used in this study, implies that 5% of the wavelet power should be above this level for each period. Following this method, the plots of 3 wavelet power spectra (WPS) were prepared for each period range separately for data series of FI on the northern and the southern hemispheres as well as on the total surface of the Sun (Figures 5–7). To provide a complete view of the temporal variability we combined the top panels of Figures 5–7 in

one figure; i.e., the whole period ranges of WPS for the total surface of the Sun is shown in Figure 8.

In comparison with the significant power peaks derived using the discrete Fourier transform (Table II) the time–period distributions of the FI WPS show extremely intermittent behavior of power at all periods. The temporal variations of power are most pronounced at those periods detected with the Fourier transform.

3. Results

In this work, the Fourier transform and the wavelet techniques are utilized to study (a) the power spectrum which provides continuous temporal evolution of the entire range of periods, (b) the time variation of power spectra for a few selected period intervals like 1500–500, 500–100, and 100–30 days, since the wavelet transform method gives detailed information on the time localization of each periodicity. We can collect these intervals as long-term (1500–500 days) and intermediate-term (500–30 days) periodicities.

3.1. Long-term periodicities

The most prominent period is the 3.1-year (1153 days) peak in the power spectrum of FI for the total surface of the Sun. The second one is the 1.7-year (618 days) peak whose significance is low in this case (Figure 2(a)). The northern-hemisphere time series of FI shows two prominent periods, which are 1.4 years (498 days) (Figure 3(b)) and 1.5 years (544 days) (Figure 2(b)) with high significance levels. Although 498 days is less than the long-term interval mentioned above, we consider it as a long-term periodicity. A close look at Figure 2(c), which illustrates the southern hemisphere time series of FI, shows three peaks which reach above 10% FAP level; these are 1.4-year (510-day), 1.5-year (539-day), and 1.8-year (661-day) periodicities. There is one more significant peak at 781 days with a 13% FAP value.

The time–period distribution of the total FI WPS (Figure 5, top panel) shows the most significant period at 2.14 years (780 days). It is completely different from the most prominent period (3.1 years), derived using the Fourier transform. The 3.1-year period is localized only to the maximum of the cycle 21 and to the ascending phase of cycle 22. The period of 2.05 years is oppositely located to the year after the maximum of the cycle 22 (1990). No final results about these periods can be drawn for cycles 20 and 23 except for the enhancement of the period of 3.8 years at the maximum of the cycle 20. The second prominent period of 1.7 years, derived using the Fourier transform, is clearly located only on the descending phase of cycle 21 (1983).

A simpler situation was found for the FI power spectra of the individual hemispheres where there is coincidence of the most significant periods, derived using the

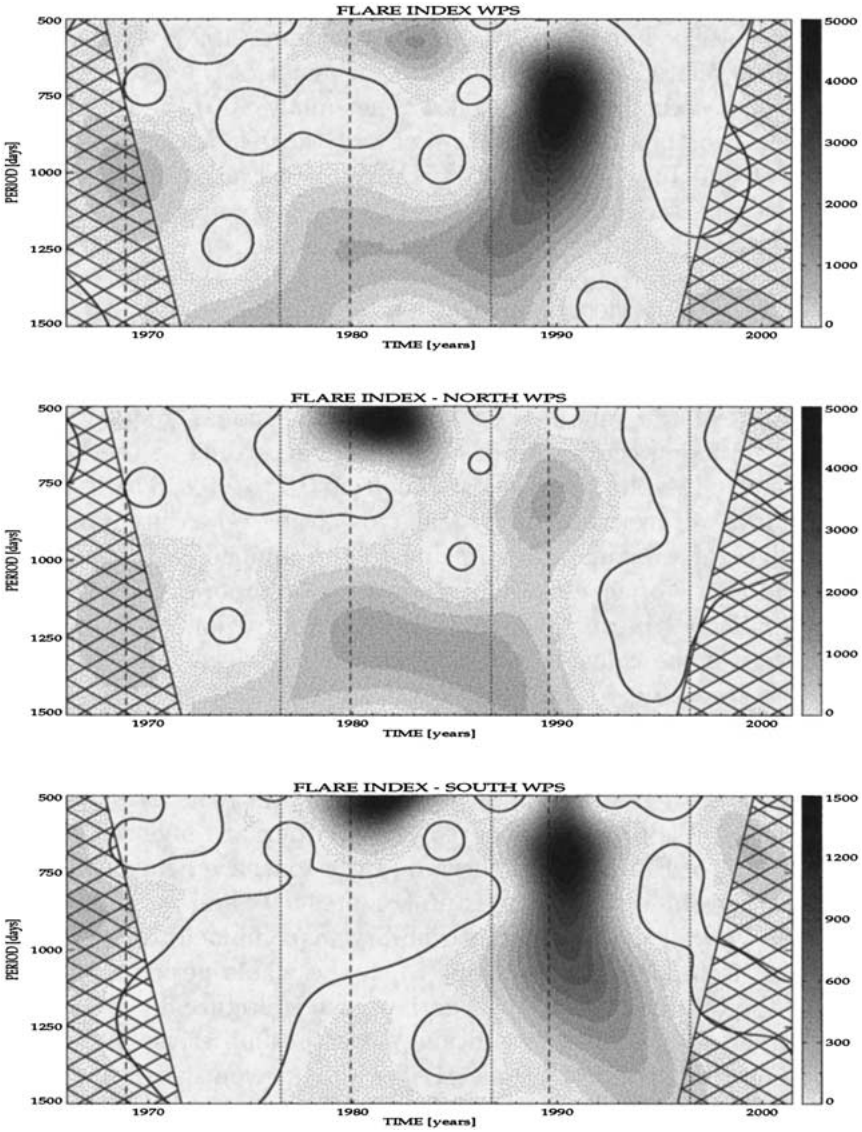

Figure 5. The wavelet power spectra of the FI time series for the period range 500–1500 days. Spectra of the FI of the total and of the northern and southern hemisphere are given in the *top*, *middle*, and *bottom panels*. Grey-scale coding of power from white to black represents the square root of power (a.u.) in a linear scale given on the right side bar. The *solid curve* shows the 95% confidence levels of the local power above the noise level assuming noise independence on periods. The cone of incidence is marked by the *cross-hatched regions. Dashed* and *dotted vertical lines* mark the solar activity cycle maxima and minima according to the Wolf's sunspot index, respectively.

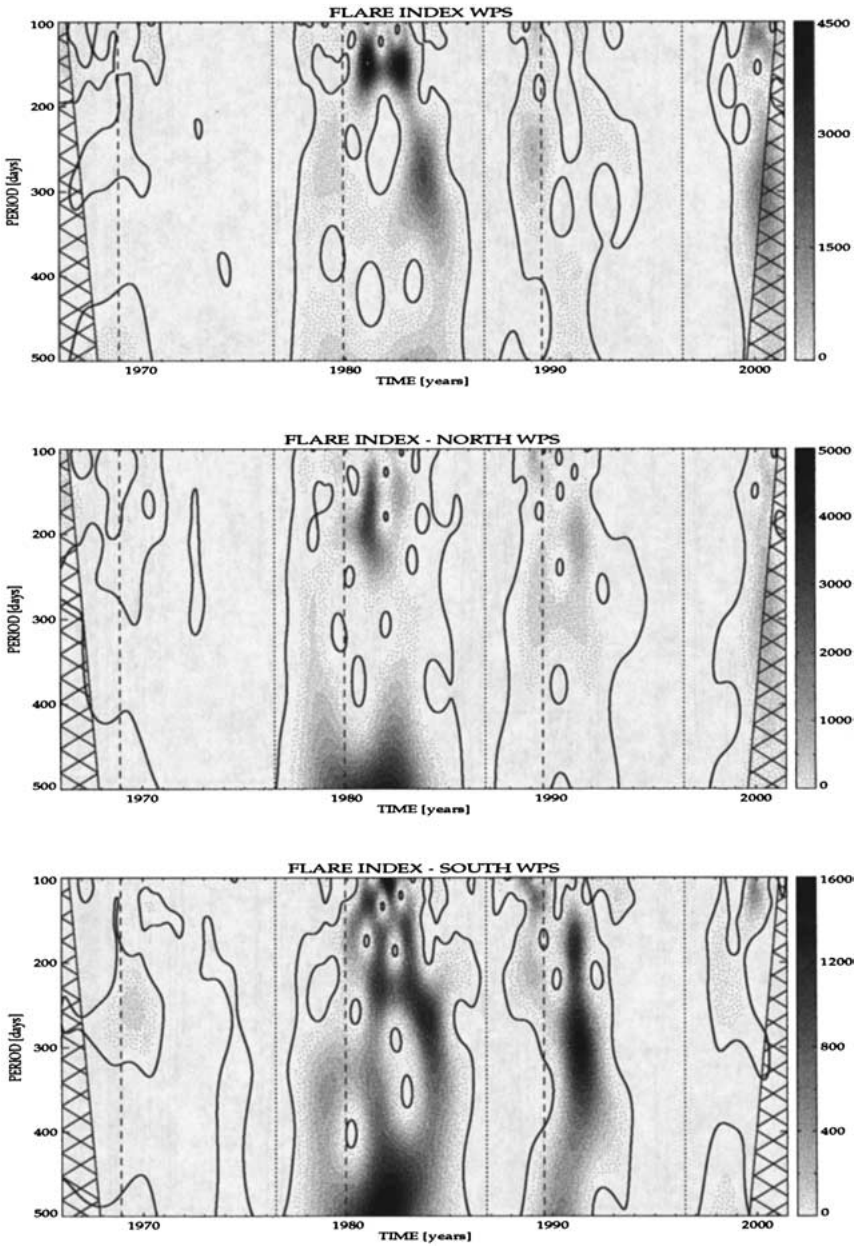

Figure 6. The wavelet power spectra of the FI time series for the period range 100–500 days. Spectra of the total FI and FI of the northern and southern hemisphere are given in the *top*, *middle*, and *bottom panels*. Grey-scale coding, *the solid curve*, *cross-hatched regions*, and *dashed* and *dotted vertical lines* are of the same meaning as in Figure 5.

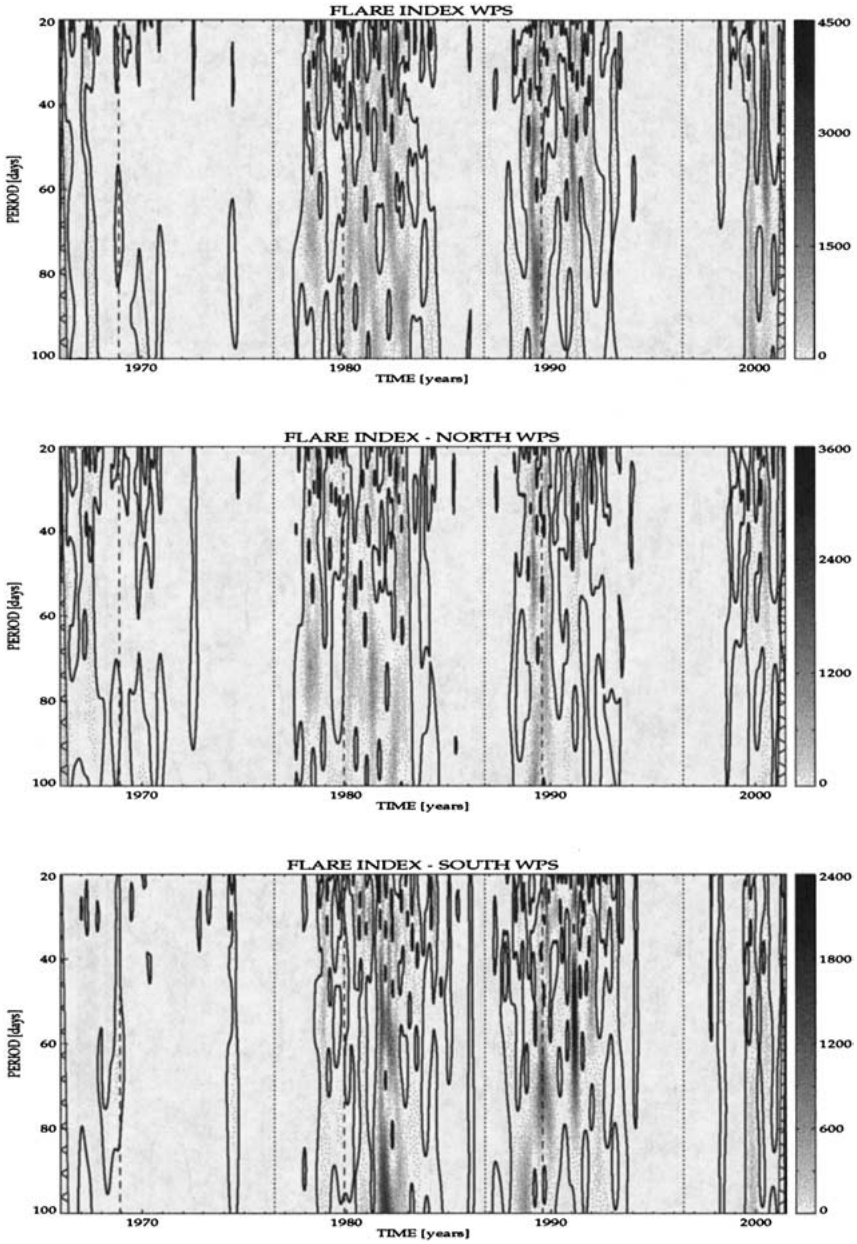

Figure 7. The wavelet power spectra of the FI time series for the period range 20–100 days. Spectra of the total FI and FI of the northern and southern hemisphere are given in the *top*, *middle*, and *bottom panels*. Grey-scale coding, the *solid curve*, *cross-hatched regions*, and *dashed* and *dotted vertical lines* are of the same meaning as in Figure 5.

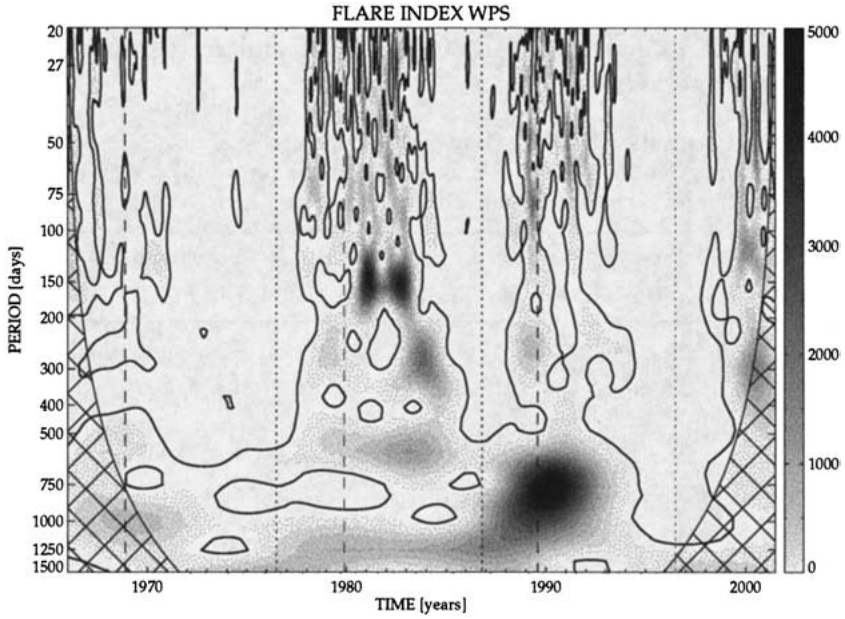

Figure 8. The wavelet power spectrum of the total FI time series for the period range 20–1500 days. Grey-scale coding, the *solid curve*, *cross-hatched regions*, and *dashed* and *dotted vertical lines* are of the same meaning as in Figure 5.

Fourier transform, with those of the wavelet transform. In the case of the northern hemisphere (Figure 5, middle panel) the periods of 498 days and 544 days are seen as the extremely enhanced power at a period around 540 days in the descending phase of cycle 21 (1980–1983). Another enhanced period of 1300 days (Figure 5, middle panel) spanning the long interval between 1979 and 1990 is a complement to the weak peak at 3.6 years obtained with the FT (Figure 2(b)). The WT power peak localized at the maximum of the cycle 22 (1989) with a period of 800 days could be seen also in the Figure 2(b) significantly weakened by the absence of that period in the rest of the FI time series.

For the southern hemisphere (Figure 5, bottom panel) the periods just above 500 days behave similarly to the northern hemisphere. The period and temporal location of the most enhanced power is the same in both hemispheres. Contrary to that behavior the period around 660 days is different between the hemispheres. Here (south) the enhancement is so high as in the case of the 500-day period and it is localized in time to the year 1990. Power at 1300 days is absent.

Summarizing the behavior of the FI in individual hemispheres shows that the location of periods around 500 days is the same, but the southern hemisphere exhibits in addition to the northern one an extreme enhancement of period at 660 days seen only in the maximum of cycle 22. The behavior of cycle 21 does not show any significant power differences between the hemispheres except the absence of the power at 1300-day period in case of the southern hemisphere.

Remarkable are some differences of the power spectra between the total and hemispheric FI. One could expect that the power spectrum of the total index will be the simple sum of power spectra of both hemisphere. Nevertheless different phases of each period under study at each hemisphere can lead to the completely different situation when, e.g., a very weak peak in the northern hemisphere and the broad weak peak in the southern hemisphere, both close to 1153 days, generate the most significant peak for the FI of the total surface. All periods found well above the given statistical levels are therefore real although this strange relation between the separate behaviour of power in separate hemispheres according to the total index is observed.

3.2. INTERMEDIATE-TERM PERIODICITIES

The power spectra of the FI of the total surface of the Sun for the intermediate-term periodicities are presented in Figures 3(a) and 4(a), with a frequency resolution of 0.89 nHz. The major periods are at 53 days and 147 days and a peak is seen around 84 days, too, but this peak is under the 10% FAP level. Figures 3(b) and 4(b) show the power spectra of the FI of the northern hemisphere of the Sun. As can be seen, the major periods are at 73 and 205 days. Additional peaks, but with bigger FAP values, are seen at 85, 193, and 220 days. The power spectra of the FI of the southern hemisphere of the Sun are illustrated in Figures 3(c) and 4(c). The prominent periods are at 54 and 116 days. The other peaks are seen around 75 and 316 days with 9.2% FAP values.

Intermediate-term WT power spectra are displayed in Figures 6 and 7 dividing the period range at 100 days. The total FI series shows that the 147-day major period, obtained by Fourier transform is localized mostly to the temporal interval on the ascending phase of the cycle 21 (1980–1983) (Figure 6, top panel). This major period has appeared in two pulses; the first one in 1980–1981 and the second one during the year 1982. Longer periods of almost 276 days (1983, 2000) and of 260 days (1989) are significant in the given years although power at these periods is of high FAP value (Figure 3(a)). The behavior at the shorter periods (Figure 7, top panel) is of highly intermittent nature. All three short periods (see Table II) can be identified during some temporal moments. Generally the pulses of power are very short thus changing the most significant period quickly in time. This fact is complementary to the relatively high number of periods of almost the same power displayed in Figure 4(a).

The WT power spectra of the FI of the northern hemisphere of the Sun (Figures 6 and 7, middle panels) show the power pattern at 150-day period shifting the period value to 200 days (1981) as well as some decrease of the power at 150 days for year 1982. The 200-day period is enhanced also in 1991 and the 300-day period at maximum and at the descending phase of cycle 22 as well as in 2000. Therefore, the decrease of power at 150 days, an enhancement of it at about 200 days, seen in results of the Fourier transform (Figure 3(b)), are confirmed by the WT results.

For periods shorter than 100 days, the results of WT (Figure 7, bottom panel) show that the 73-day period is localized in years 1978, 1981–1982, and 1989.

The southern hemisphere FI WPS (Figures 6 and 7, bottom panels) confirm the most significant period of 116 days but located mostly in the year 1982. Other intermediate-term periodicities are: 250 days in 1981, 280 days in 1984 and 180 and 300 days in 1990–1991. These periods are notable also in the Fourier power spectra but all of higher FAP values. The two shorter period 75- and 54-day periods are localized strongly to the years 1981–1982 and 1990–1991, but the latter one is very strong especially in the first part of the year 1991. These two periods are also detected by Fourier transform with quite good FAP values.

3.3. Hemispheric (N-S) asymmetry of flare index

The results of this work clearly demonstrate that there exists a hemispheric asymmetry in term of flare index. However, using the north-south asymmetry of the FI, Özgüç and Ataç (1996) have confirmed the existence of the 25.5-day fundamental period (Bai and Sturrock, 1991) of the Sun. Ataç and Özgüç (1998, 2001) have examined this asymmetry for the cycle 22 and for the rising part of cycle 23, separately. In Figure 9 this asymmetry is plotted for the whole studied period using 5-month running means of the FI. To show the different behavior of the FI between the two hemispheres clearly we filled the area of the northern hemisphere values. One can easily see that the flare activity begins earlier in the northern hemisphere in cycles 20 and 21. But contrary to the previous two cycles it begins earlier in the southern hemisphere in cycles 22 and 23. The dominance of the flare activity was in favour of the northern hemisphere for the ascending parts of cycles 20 and 21, while it showed a drift behavior between the two hemispheres during the ascending parts of cycles 22 and 23. We may also state that this dominance turned to the southern hemisphere during the descending parts of cycles 20–22. Therefore we may expect that during the descending part of cycle 23 the flare activity will be dominant in the southern hemisphere.

To compare the N–S asymmetry of the FI with another activity index we added a plot to Figure 9 using 5-month running means of the total sunspot area (in millionths of solar hemisphere) time series. We see that the N–S asymmetry shows similar behavior for the total areas of sunspot groups.

4. Discussion

The goal of understanding any periodic variation in solar activity records, that may be indicative of true solar cyclicity, lies in the practical need to characterize quantitatively those sources of variance that are potential tools for predicting future solar activity. Therefore, we have studied temporal variations of the flare index considering the FI for the period 1966–2001. We examined, in the FI data, the

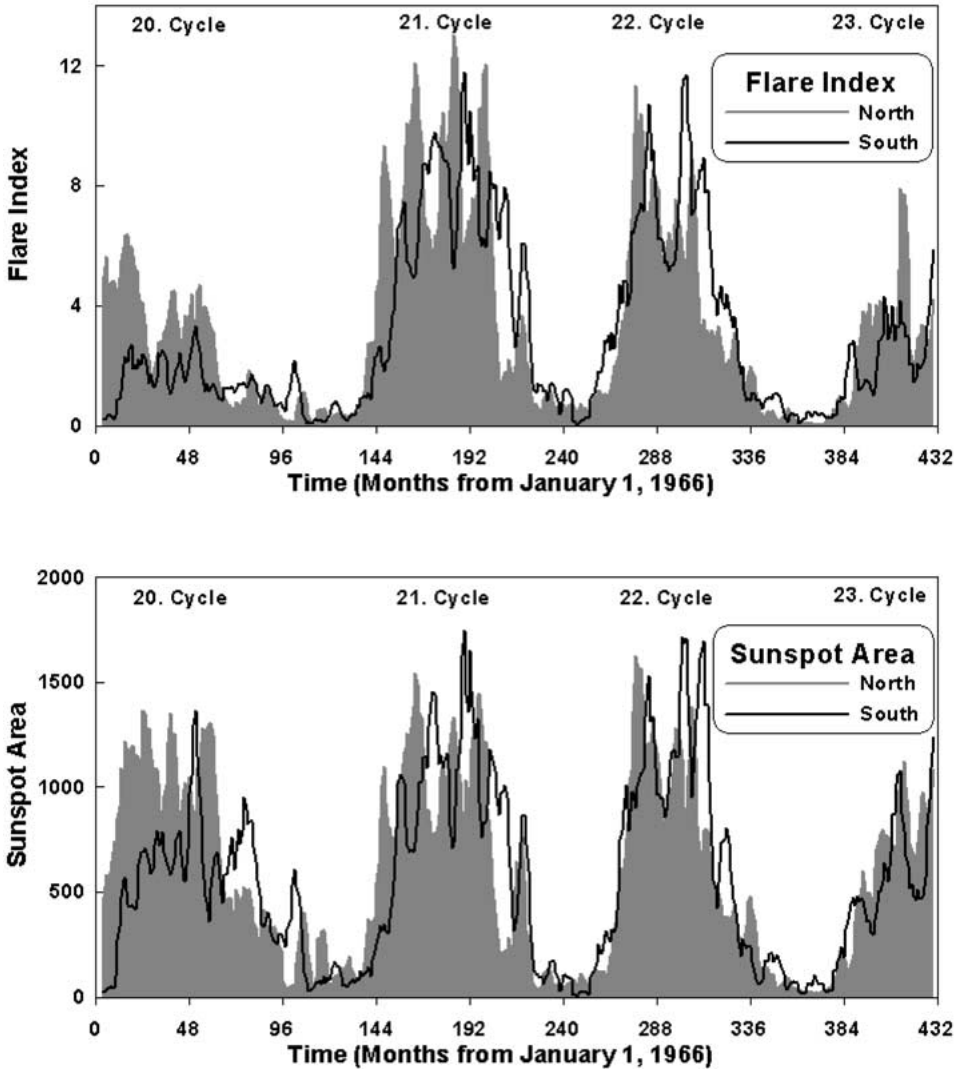

Figure 9. Five-month running mean plots of the northern and the southern hemispheres' FI and sunspot area time series between 1 January 1966 to 31 December 2000. Unit of the sunspot area is millionths of solar hemisphere. *Filled areas* demonstrate the northern hemisphere values.

reality of solar periodicities concentrating on periods between 30 and 1500 days. During this time period, the FI shows many periodicities listed in Table II.

A 540-day periodicity has been found before by Akioka *et al.* (1986) for TA (sum of maximum areas of sunspot groups per solar rotation) and MA (mean area of sunspot groups per solar rotation), during cycle 21. In FI power spectra, this periodicity has a significant peak when both hemispheres are considered separately during the years 1981–1982 (Figures 6 and 7, top panels). However, Oliver,

Carbonelli, and Ballester (1992) found no evidence for this period in their power spectrum of Zürich sunspot number and sunspot areas during cycle 21.

Recently, it is reported that the solar rotation rate of the Sun near the base of its convective zone changes with a period of roughly 1.3 years (Howe *et al.*, 2000); very recently, using wavelet analysis of sunspot areas and sunspot numbers, Krivova and Solanki (2002) concluded that the periodicity of 1.3 years revealed in the rotation rate of the Sun at the base of convection zone is also present in these records of solar activity. In our analysis we found this period as 1.36 years (498 days) both in FT and WT during the years 1981–1982 but only when both hemispheres are considered separately. However, Hady (2002) has also reported that the 1.36 years periodicity exists in the power spectrum of the 10.7 cm radio flux of the ascending branch of cycle 23. In their analysis of the area and numbers of sunspot groups from 1969 to 1986, Akioka *et al.* (1987) detected this periodicity near 510 days (1.4 years). This periodicity at 1.3 years has also been detected in variations of geomagnetic activity and interplanetary magnetic field (Paularena, Szabo, and Richardson, 1995; Szabo, Lepping, and King, 1995; Lockwood, 2001). According to the recent analysis of Lockwood (2001), the period was found to be quite prominent for the interval 1995–2000.

Oliver, Carbonelli, and Ballester (1992) found that a significant peak at 322 days appears in the Zürich sunspot number and at 316 days in sunspot areas for cycle 21. This is the same peak found, during cycle 21, by Lean and Brueckner (1989) for the sunspot blocking function, by Delache, Laclare, and Sadsaoud (1985) in solar diameter measurements and by Rybák, Antalová and Storini, (2000) in the non-flare full-disk soft X-ray background. However we can detect this periodicity only in the southern hemisphere FI power spectrum for cycle 22 as 316 days (Figure 7, middle panel). For the northern hemisphere this peak is seen as 301 days with a less significance (more than 10% FAP).

Comparing the values of periods, determined by WT, to the temporal interval length when the power is enhanced, it is clearly seen that the 'signal' is strongly intermittent. This should be transformed to the language of the Sun. Recently, Lou (2000) reported that these quasi periodicities seen in solar flare activities are most likely related to large-scale equatorial trapped Rossby-type waves in the solar photosphere. After analyzing the FI time series, we find that episodes of the 147-day periodicity occurred around the maxima of cycles. In order to distinguish between the wavelet power around the 140–170 days oscillations, the temporal evolution of wavelet power corresponding to 140–170 days periods in FI are plotted separately in Figure 10. The wavelet power of this oscillation peaks around the early declining phase of cycles 21 and 22, with the magnitude of peak values changing from one cycle to the next. In contrast it peaks just before the maxima of cycles 20 and 23 (Figure 10). These episodes may be useful for a theoretical understanding of these kind of periodicities since it was long overdue.

The investigation confirms that many of these periods are intermittent. Ruzmaikin (2001) brings an explanation that the magnetic fields emerge at the solar

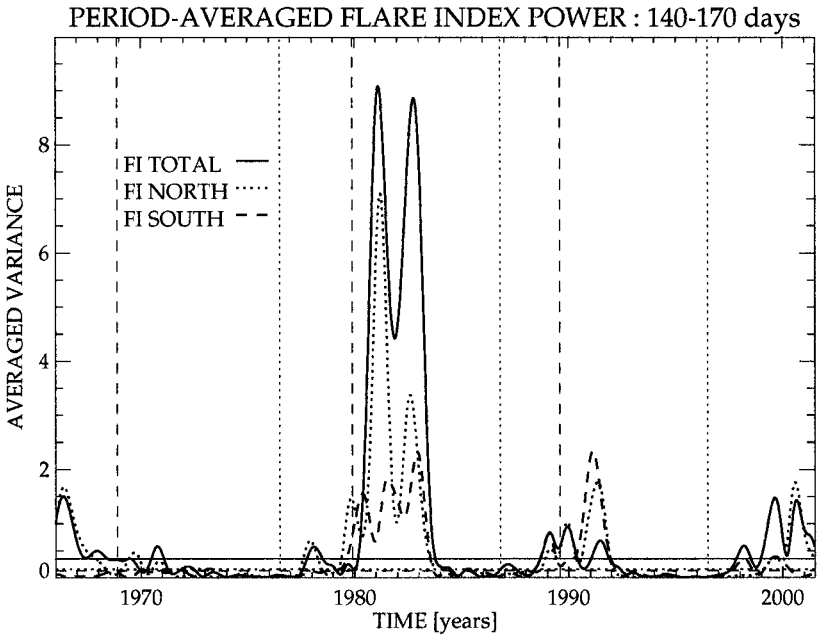

Figure 10. Behavior of the period-averaged WT power of the intermediate-term periods (140–170 days). The *dashed-dotted horizontal lines* show 95% confidence levels of these period-averaged power spectra. Solar activity maxima and minima are marked with the *dashed* and the *dotted lines*, respectively.

surface at random times and places when the total magnetic field (mean field plus a fluctuation) exceeds the threshold for buoyancy. In this way the mean field is responsible for the observed regularities of the sunspot magnetic fields, such as Hale's law and the 11-year periodicity, and the fluctuating fields are responsible of emergence of individual flux tubes then merging into sunspots.

Besides these periodicities, 73- and 53-day periodicities are found by our analysis. These two periodicities also show episodes before and after maxima of cycles 21, 22, and 23. No evidence of these two is found for cycle 20. The general suggestion is that these variations are related to differences in the internal flows (e.g., differential rotation and meridional flow) and the magnetic field itself (e.g., polar field strength) of each cycle.

Using the sunspot blocking function, Ca II K plage index and radio flux data which reflect different solar activity region phenomena, Lean and Brueckner (1989) found 162, 270, 287, and 390 days periods. In our analysis we could not find any evidence for these periods. Some major periods seen in the other activity indices (in sunspot number or areas) may not be detected in the FI; Ballester, Oliver, and Baudin (1999) put forward a hypothesis that when the periodicity appears in sunspot areas only, i.e., when the magnetic flux emerges mostly within already formed active regions, a similar periodicity should appear in high-energy solar

flares. To the contrary, when the periodic emergence of magnetic flux is produced in the form of new and scattered sunspot groups, no periodicity should appear in energetic solar flares due to the small magnetic complexity of sunspot groups.

Acknowledgements

The grouped flare lists were made available by E. H. Erwin of WDC-A for Solar-Terrestrial Physics. The wavelet transform algorithm of C. Torrence and G. P. Compo, available at *http://paos.colorado.edu/ research/wavelets/* has been used in this work. The authors thank to the referee for the constructive comments. This work was supported by Boğaziçi University Research Fund by the project of 00T101 and by the Slovak grant agency VEGA by the grant 2/3015/03.

References

Akioka, M., Kubata, J., Suzuki, M., Ichimoto, K., and Tohmura, I.: 1987, *Solar Phys.* **112**, 313.
Ataç, T.: 1987, *Astrophys. Space Sci.* **135**, 201.
Ataç, T. and Özgüç, A.: 1998, *Solar Phys.* **180**, 397.
Ataç, T. and Özgüç, A.: 2001, *Solar Phys.* **198**, 399.
Bai, T.: 1992, *Astrophys. J.* **397**, 584.
Bai, T. and Cliver, E. W.: 1990, *Astrophys. J.* **363**, 299.
Bai, T. and Sturrock, P. A.: 1987, *Nature* **327**, 601.
Bai, T. and Sturrock, P. A.: 1991, *Nature* **352**, 360.
Ballester, J. L., Oliver, R., and Baudin, F.: 1999, *Astrophys. J.* **522**, L153.
Bloomfield, P.: 1976, *Fourier Analysis of Time Series: An Introduction*, John Wiley and Sons, New York.
Bogart, R. S. and Bai, T.: 1985, *Astrophys. J.* **229**, L51.
Caballero, R. and Valdés-Galicia, J. F.: 2001, *Adv. Space Res.* **27**, 583.
Daubechies, I.: 1990, *IEEE Transactions on Information Theory* **36**, 961.
de Jager, O. C.: 1987, Ph. D. Thesis, Potchefstroom University, Potchefstroom.
Delache, P., Laclare, F., and Sadsaoud, H.: 1985, *Nature* **317**, 416.
Dennis, B. R.: 1985, *Solar Phys.* **100**, 465.
Dröge, W., Gibbs, K., Grunsfeld, J. M., Meyer, P., and Newport, B. J.: 1990, *Astrophys. J. Suppl.* **73**, 297.
Hady, A. A.: 2002, *Planet. Space Sci.* **50**, 89.
Horne, J. H. and Baliunas, S. L.: 1986, *Astrophys. J.* **302**, 757.
Howe, R., Christensen-Dalsgaard, J., Hill, F. *et al.*: 2000, *Science* **287**, 2456.
Joshi, A.: 2001, *Solar Phys.* **198**, 149.
Kane, R. P.: 2002, *Solar Phys.* **207**, 17.
Kleczek, J.: 1952, *Publ. Czech Centr. Astron. Inst.*, No. 22.
Krivova, N. A. and Solanki, S. K.: 2002, *Astron. Astrophys.* **394**, 701.
Kumar, P. and Faufoula-Georgiou, E.: 1997, *Rev. Geophys.* **35**, 385.
Lean, J. and Brueckner, G. E.: 1989, *Astrophys. J.* **337**, 568.
Li, K. J., Wang, J. X., Xiong, S. Y., Liang, H. F., Yun, H. S., and Gu, X. M.: 2002, *Astron. Astrophys.* **383**, 648.
Lockwood, M.: 2001, *J. Geophys. Res.* **106**, 16021.

Lou, Y.: 2000, *Astrophys. J.* **540**, 1102.
Oliver, R., Carbonelli, M., and Ballester, J. L.: 1992, *Solar Phys.* **137**, 141.
Oliver, R., Ballester, J. L., and Baudin, F.: 1998, *Nature* **394**, 552.
Özgüç, A. and Ataç, T.: 1989, *Solar Phys.* **123**, 357.
Özgüç, A. and Ataç, T.: 1994, *Solar Phys.* **150**, 339.
Özgüç, A. and Ataç, T.: 1996, *Solar Phys.* **163**, 183.
Özgüç, A., Ataç, T., and Rybák, J.: 2002, *J. Geophys. Res*. **107**, 10.1029/ 2001JA009080.
Özgüç, A., Tulunay, Y., and Ataç, T.:1998, *Adv. Space Res.* **22**, 139.
Özgüç, A., Ataç, T., Tulunay, Y., and Stanislavska, I.: 1998, *Studia Geophys. Geod.* **42**, 112.
Paularena, K. I., Szabo, A., and Richardson, J. D.: 1995 , *Geophys. Res. Lett.* **22**, 3001.
Rieger, E., Share, G. H., Forrest, D. J., Kanbach, G., Reppin, C., and Chupp, E. L.: 1984, *Nature* **312**, 623.
Ruzmaikin, A.: 2001, *Space Sci. Rev.* **95**, 43.
Rybák, J., Antalová, A., Storini, M.:2000, in A. Wilson (ed.), *The Solar Cycle and Terrestrial Climate*, ESA SP-463, 419.
Scargle, J. D.: 1982, *Astrophys. J.* **263**, 835.
Szabo, A., Lepping, R. P., and King, J. H.: 1995, *Geophys. Res. Lett.* **22**, 1845.
Torrence, C. and Compo, G. P.: 1998, *Bul. Am. Meteor. Soc.* **79**, 61.
Tripathy, S. C., Kumar, B., Jain, K., and Bhatnagar, A.: 2000, *J. Astrophys. Astron.* **21**, 357.
Veretenenko, S. V. and Pudovkin, M. I.: 1999, *J. Atmospheric Solar-Terrest. Phys.* **61**, 521.
Verma, V. K., Joshi, G. C., Uddin, W., and Palival, D. C.: 1991, *Astron. Astrophys.* **90**, 83.